3812

NASA Technical Memorandum 109045

Low-Speed Longitudinal Aerodynamic Characteristics of a Flat-Plate Planform Model of an Advanced Fighter Configuration

B. E. McGrath, and D. H. Neuhart
Lockheed Engineering and Sciences Co., Hampton, Virginia

G. M. Gatlin
Langley Research Center, Hampton, Virginia

P. O'Neil
McDonnell Douglas Aerospace, St. Louis, Missouri

March 1994

National Aeronautics and
Space Administration
Langley Research Center
Hampton, Virginia 23681-0001

LOW-SPEED LONGITUDINAL AERODYNAMIC CHARACTERISTICS OF A FLAT-PLATE PLANFORM MODEL OF AN ADVANCED FIGHTER CONFIGURATION

B. E. McGrath
D. H. Neuhart
Lockheed Engineering and Sciences Co.

G. M. Gatlin
NASA Langley Research Center

and

P. O'Neil
McDonnell Douglas Aerospace

Abstract

A flat-plate wind tunnel model of an advanced fighter configuration was tested in the NASA Langley Subsonic Basic Research Tunnel and the 16- by 24-Inch Water Tunnel. The test objectives were to obtain and evaluate the low-speed longitudinal aerodynamic characteristics of a candidate configuration for the integration of several new innovative wing designs. The flat plate test allowed for the initial evaluation of the candidate planform and was designated as the baseline planform for the innovative wing design study. Low-speed longitudinal aerodynamic data were obtained over a range of freestream dynamic pressures from 7.5 psf to 30 psf (M = 0.07 to M = 0.14) and angles-of-attack from 0° to 40°. The aerodynamic data are presented in coefficient form for the lift, induced drag and pitching moment. Flow-visualization results obtained were photographs of the flow pattern over the flat plate model in the water tunnel for angles-of-attack from 10° to 40°. The force and moment coefficients and the flow-visualization photographs showed the linear and nonlinear aerodynamic characteristics due to attached flow and vortical flow over the flat plate model. Comparison between experiment and linear theory showed good agreement for the lift and induced drag; however, the agreement was poor for the pitching moment.

Nomenclature

All measurements are presented in U.S. customary units. All data have been reduced to standard coefficient form, and longitudinal data are presented in the stability axes system.

AR Aspect ratio, $\frac{b^2}{S}$

a	Speed of sound, $\sqrt{\gamma RT}$, ft/sec
b	Wing span, in
$\check{c}$	Mean aerodynamic chord, in
c_r	Wing root chord, in
c_t	Wing tip chord, in
C_A	Axial force coefficient, $\frac{\text{axial force}}{qS}$
C_D	Drag coefficient, $\frac{\text{drag}}{qS}$
$C_{D,0}$	Zero-lift drag coefficient
$C_{D,i}$	Induced drag coefficient
C_L	Lift coefficient, $\frac{\text{lift}}{qS}$
C_m	Pitching moment coefficient, $\frac{\text{pitching moment}}{qS\check{c}}$
C_N	Normal force coefficient, $\frac{\text{normal force}}{qS}$
$\frac{dC_M}{dC_L}$	Longitudinal stability parameter at $C_L = 0°$
M	Mach number, $\frac{V}{a}$
q	Dynamic pressure, $\frac{1}{2}\rho V^2$, lbs/ft^2 (psf)
R	Specific gas constant
S	Reference area, ft^2

T	Absolute temperature
V	Velocity, ft/sec
α	Angle-of-attack, degrees
β	Angle-of-sideslip, degrees
γ	Ratio of specific heats
Λ	Wing sweep angle, degrees
λ	Wing taper ratio, $\frac{c_t}{c_r}$
ρ	Density, slugs/ft^3

Subscripts

∞	Free-stream flow conditions
e	Wing exposed area
LE	Leading edge
r	Root
T	Total model planform area
TE	Trailing edge
t	Tip

Introduction

A flat-plate wind tunnel model of an advanced fighter configuration was fabricated and tested in the NASA Langley Subsonic Basic Research Tunnel (SBRT) and the 16- by 24-Inch Water Tunnel. The test objectives were to obtain and evaluate the low-speed longitudinal aerodynamic characteristics of a candidate configuration for the application and integration of several innovative wing designs. The planform tested was developed under the Aero Configuration/Weapons Fighter Technology (ACWFT) contract (Contract No. F33615-89-C-3004) by McDonnell Douglas Aerospace, St. Louis, for Wright Laboratories of the United States Air Force. The contractual designation of this planform is concept number 296-1204. The ACWFT planform was a good candidate for testing because a complete systems integration study had been performed which could then be applied to the integration of the innovative wing designs. Along with the systems studies, a fully three-dimensional wind tunnel model of the ACWFT (296-1204) was being designed and manufactured. A flat plate model of the ACWFT configuration was fabricated to study the integration of the innovative wing designs with the ACWFT configuration. The ACWFT planform was designated as the baseline or reference planform. Testing in SBRT and the water tunnel provided the opportunity to quickly obtain data that defined the low-speed longitudinal aerodynamic and flow field characteristics of the ACWFT (baseline) planform. Testing in these two facilities allows for greatly simplified model fabrication and data acquisition.

Low-speed longitudinal aerodynamic data were obtained on the ACWFT planform and a modified ACWFT planform. Data were collected for variations in freestream dynamic pressure from 7.5 psf to 30 psf and for angles-of-attack from 0° to 40°. This report presents aerodynamic data in coefficient form of the lift, induced drag and pitching moment for both the ACWFT and the modified ACWFT planforms. Flow-visualization photographs showing the flow patterns over the ACWFT planform at α = 10°, 20°, 30° and 40° are presented in this report.

Model Description

The geometric characteristics of the Aero Configuration/Weapons Fighter Technology (ACWFT) flat-plate wind and water tunnel models are shown in figure 1. The baseline planform model was designated as ACWFT1, and the modified planform was designated as ACWFT2. These planforms are shown in figures 1a and 1b, respectively. The flat plate models were machined from 0.063 inch-thick aluminum sheets. The planforms were finished to the proper shape by filing and smoothing the edges by hand. Planform edges were left thick and not beveled to a sharp edge. The planform modification to the ACWFT2 model was the removal of the aft body flaps; otherwise, the models are geometrically the same. The wing planform geometric

characteristics are presented in table I. The values of reference area, mean aerodynamic chord and other wing refence quantities are given in table I. These reference quantities were used for calculating the force and moment coefficients of both planform models.

The flat plate models were fixed to the upper surface of a 0.25 inch-thick aluminum plate for rigid support and attachment to the centerbody balance housing. The aluminum plate was of arbitrary shape with the edges of the lower surface beveled to a sharp edge. The centerbody balance housing contained the six-component strain-gage balance for measurement of the aerodynamic forces and moments.

Test Conditions and Techniques

Wind Tunnel

Force and moment testing of the ACWFT flat-plate wind tunnel models were conducted in the Subsonic Basic Research Tunnel (SBRT) at the NASA Langley Research Center. A photograph of the ACWFT1 model in the SBRT test section is shown in figure 2. SBRT is a continuous, open circuit, atmospheric wind tunnel capable of a maximum freestream dynamic pressure of 45 psf (V_∞ = 194 ft/sec). The tunnel test section is rectangular in shape and measures 22.5 inches wide by 32.25 inches tall with 1.45 inch by 1.45 inch corner fillets and is 73 inches in length. The cross sectional area of the test section is 5.01 ft^2. The upstream diffuser has a contraction ratio of 5.99, and the upstream entrance of the diffuser has a series of screens and honeycomb used for straightening the air flow. The fan is downstream of the test section and draws the air flow through the tunnel circuit. A calibration of the SBRT was performed under NASA Langley contract L-17886c by P. S. Barna in July 1988 and was documented in an unpublished report. The model support system is shown in figure 3 and positions the model along the tunnel centerline. The support system maintains the balance center on the tunnel centerline for the entire angle-of-attack range. The support system angle-of-attack range is from 0° to 70°. and the support system angle-of-attack can in varied in 5° increments. Figure 4 shows details of the model balance housing that was used for the ACWFT flat plate test. Table II shows the test conditions for the ACWFT flat plate test.

Data were obtained at three different values of freestream dynamic pressure to evaluate the effects of freestream dynamic pressure. The nominal test conditions were at a freestream dynamic pressure of 30 psf which corresponds to a freestream Reynolds number of 1.0×10^6 /ft and an angle-of-attack range from 0° to 40°. The force and moment balance used in the test was designated as SWT-01 and is a standard NASA Langley six-component strain-gage balance. Table III shows the maximum load capability and measurement accuracy (no worse than 0.3% of

maximum loads) in coefficient form for the normal, axial and pitching-moment channels of the balance at q_∞ = 30 psf. Even though all six components of the balance were measured only the longitudinal components were of interest in this study; therefore, only these components will be presented. Lateral/directional effects were not investigated due to the flat-plate nature of the models. All testing was conducted at zero sideslip.

Water Tunnel

The flow-visualization data were obtained in the NASA Langley 16- by 24-Inch Water Tunnel (Ref. 1). The water tunnel is a closed return tunnel with the test section measuring 16 by 24 inches and 54 inches in length and made of clear acrylic sheets to maximize visual access. The water flows vertically downward through the test section and freestream speeds between 0 and 0.75 ft/sec are obtainable. The angle-of-attack mechanism is capable of a range of angles between -33° and 33°. With the use of an offset sting, the ±33° angle-of-attack range can be shifted up to 62°. Red, green and blue vegetable dyes are injected through orifices located on the model surface to obtain visual and photographic documentation of the flow pattern over the model. The dye tube orifices on the ACWFT model were located on the lower surface along the leading edges of the planform model, and the locations of these dye tube orifices are specified on the model planform shown in figure 1a. The nominal conditions for the ACWFT test were a freestream speed of 0.25 ft/sec and an angle-of-attack range from 0° to 40°. The flow-visualization photographs were obtained with a Hasselblad camera mounted on a tripod exterior to the test section. It should be noted that the side-view photographs presented were not taken simultaneously with the top-view photographs

Results

Wind Tunnel

Force and moment data were obtained in the SBRT for two different flat plate models of the ACWFT planform. The two planforms were designated as ACWFT1 and ACWFT2 and are shown in figure 1. The data were obtained at three different values of the freestream dynamic pressure, 7.5 psf, 15 psf, and 30 psf. The data for the longitudinal aerodynamic characteristics are tabulated in table IV. The calculated values of the linear aerodynamic characteristics using the SBRT data of the ACWFT planforms are presented in table V. For comparison, table VI shows the calculated values of the linear aerodynamic characteristics using linear theory (Refs. 2 - 4) for the ACWFT1 planform. The aerodynamic data are plotted in figures 5 through 7 as a function of α for the lift and

pitching moment coefficients, and as function of C_L for the induced drag coefficient. Data for three values of q_∞ are presented for the ACWFT1 flat-plate model and only one value of q_∞ for the ACWFT2 flat-plate model. The pitching moment reference center was at 25 percent of $\bar{c}$ (see figure 1), and the induced drag was obtained by subtracting out the value of C_D at $\alpha = 0°$ from the total value of drag at each α. A comparison between the aerodynamic data and linear theory is presented in figures 8 through 10.

The lift coefficient data for the ACWFT1 planform, presented in figure 5, shows a small variation of lift as a function of q_∞ up to $\alpha = 30°$. For $\alpha > 30°$, the lift coefficient does not vary with q_∞. The ACWFT1 data also shows the nonlinear increase in lift due to vortex lift effects for $\alpha > 10°$. The ACWFT2 planform was only tested at $q_\infty = 30$ psf, and the lift data for this planform show similar characteristics when compared to ACWFT1. The ACWFT2 planform is nearly identical to the ACWFT1 planform except for the removal of the aft body flaps. With only this small geometric difference, the lift characteristics of each planform should be and are similar to one another, except for $\alpha > 25°$. The induced drag characteristics for the ACWFT1 planform show very small effects of q_∞. The induced drag characteristics of the ACWFT2 planform are very nearly the same as for the ACWFT1 planform, except for $C_L > 1.25$ where the induced drag coefficient at a given C_L for ACWFT2 is higher than for ACWFT1. The pitching moment data shows that both ACWFT planforms were unstable for the entire α range. The ACWFT2 planform was slightly more unstable in pitch than the ACWFT1 planform because of the reduction in total planform area. This area reduction provided for a smaller nose down pitching moment contribution by the aft end of the ACWFT2 planform. The ACWFT1 data shows that pitching moment was nearly independent of q_∞ for $\alpha \leq 15°$; however, for α between 15° and 40°, the magnitude of the pitching moment decreases (becomes more stable) as q_∞ decreases for a given angle-of-attack.

Comparisons between the SBRT data and linear theory (Refs. 2 - 4) for the ACWFT1 planform are shown in figures 8, 9 and 10 for the lift, induced drag and pitching moment coefficients, respectively. The linear theory results shown were calculated for three different leading-edge flow conditions, no leading-edge thrust, full leading-edge thrust and attainable leading-edge thrust. Each of these conditions is a different accounting of the leading-edge vortex or thrust effects on the lift, drag and pitching moment. The comparison of the linear aerodynamic characteristics between the SBRT data (table V) and linear theory (table VI - attainable thrust) shows that the lift curve slope, C_{L_α}, and the longitudinal stability parameter, dC_m/dC_L agree to within 15 percent of one another, respectively. Further examination of the SBRT data and linear theory comparison shows that the calculation for lift with attainable thrust agrees best with the SBRT data up to $\alpha = 25°$. For $\alpha > 25°$, the flow field is dominated by vortex flow and the onset of vortex burst that causes highly nonlinear aerodynamic characteristics and are not modeled by linear theory. One observation worth discussion is that the SBRT lift data does not exactly pass

through zero at $\alpha = 0°$. For an infinitely thin flat plate, the lift would exactly pass through zero at $\alpha = 0°$; however, the actual models have thickness and a small amount of negative camber due to thickness. Thus, the lift has a small non zero value at $\alpha = 0°$. The induced drag comparison again shows that linear theory with attainable thrust agrees well the SBRT data. Breakdown in agreement between linear theory and experiment of the induced drag occurs at a high lift coefficient or high angle-of-attack where the flow field is dominated by vortex flow and the onset of vortex burst. The pitching moment comparison between SBRT data and linear theory is much less favorable. The initial slope and direction of the pitching moment agree reasonably well, but the magnitude of the pitching moment is significantly under predicted by linear theory. In addition, linear theory did not calculate the same trends for pitching moment as a function of α.

The reason for including a comparison of the SBRT data to linear theory was to provide additional confidence in the data obtained in SBRT for the ACWFT planforms. The above comparisons with linear theory show that the SBRT data agrees well for lift and induced drag. However, the comparison with pitching moment was poor, but typical for linear theory results (Refs. 2 - 4). Other disagreements between theory and experiment were at flow conditions where the nonlinear aerodynamic characteristics of vortex flow and vortex burst dominate and one would not expect good agreement.

Water Tunnel

The photographic data obtained in the NASA Langley 16- by 24-Inch Water Tunnel was for the ACWFT1 planform. The same flat plate model that was tested in SBRT was used in the water tunnel test. Dye tubes were attached to the underside of the planform with the tube orifices positioned along the edge of the planform at three different axial locations. The approximate axial locations of dye tube orifices are indicated in figure 1a. The dye tubes were positioned symmetrically about the axial centerline of the planform. To visualize the flow pattern about the ACWFT1 planform, red, green and blue vegetable dyes were injected out of the tube orifices located at the forebody tip, mid-forebody and forebody/wing leading-edge intersection, respectively. The flow patterns typically traced out by the dye are the forebody and wing vortices including vortex bursting. Specific characteristics of these flow patterns that can be observed in the water tunnel are the onset of vortex formation, vortex asymmetry, vortex burst, vortex dynamics and separated and reattached flow (Refs. 5 and 6). Photographic data obtained for the ACWFT1 planform consisted of top and side views of the flow pattern at $\alpha = 10°$, 20°, 30° and 40°. These photos are presented and figures 11 through 14.

Figures 11a and 11b show the top and side view of the flow pattern over the ACWFT1 planform at $\alpha = 10°$. The top view shows that a pair of vortices form at the tip of the forebody. The

swirling nature of the red dye visualizes the location and direction of the core of each vortex in the forebody vortex pair. The green dye also visualizes the forebody vortex pair; however, the location of the dye tube orifice allows the dye to be injected into the flow so that the dye shows the size, shape and location of each vortex at a larger vortex radial position. The diffuse nature of both the red and green dyes suggests that this vortex pair was relatively weak at this α. The vortex pair exists over the entire length of the planform and does not burst until well beyond the aft end of the planform. The blue dye shows the flow pattern near the forebody/wing leading-edge intersection. The slight swirling and relatively diffuse nature of the blue dye suggest that a very weak vortex formed over the wing with vortex bursting occurring near 25 percent of $\bar{c}$. The top photo also shows the variation of the spanwise location of the forebody and wing vortices with respect to each other. The forebody vortex pair generally remains inboard over the planform until the wing vortex bursts and then each vortex in the forebody vortex pair moves outboard over the wing probably due to the presence of the centerbody and eventually follows the outboard side edge of the afterbody portion of the planform. The side view photo shows the extent or height above the planform surface of the vortices just discussed. The side view photos do not show the same detail as the top view photos; therefore, not as much discussion will be devoted to them. For $\alpha = 10°$, the side view shows the flow reattaching to the wing surface (blue dye) downstream of vortex burst.

Figures 12a and 12b show the top and side view of the flow pattern over the ACWFT1 planform at $\alpha = 20°$. Observing the tight swirling nature of the red and green dye that define the vortex core and size, the top view photo shows that the forebody vortex pair has become well defined and stronger. The wing vortices do not appear to strengthen with an increase in α, but remain very similar in size and structure as compared to the $\alpha = 10°$ results. The outboard shift in the forebody vortex pair again occurs just downstream of the bursting location of the wing vortex. As each vortex of the forebody vortex pair moves outboard to the fuselage/wing trailing edge intersection, an asymmetric oscillatory location of burst was exhibited. The asymmetric oscillatory location of burst means that the axial location of burst moved a large distance both upstream and downstream in a continuous oscillation and did so in an asymmetric manner for each vortex of the forebody vortex pair. Vortex burst and location of burst considerably effect the lift and pitching moment of the configuration. Vortex burst is a highly nonlinear effect that reduces lift and influences the magnitude and direction of the pitching moment while occurring at a position over top of the configuration planform. At $\alpha = 20°$, the lift and pitching moment coefficients of the ACWFT1 planform begin to show the nonlinear influences of vortex burst and burst location. The side view shows that the height of the vortical flows above the model surface increases as α increases.

Figures 13a and 13b show the top and side view of the flow pattern over the ACWFT1 planform at $\alpha = 30°$. The red and green dyes again define the forebody vortex pair. The most significant observation is that the location of burst of the forebody vortex pair moved forward to a position close to 50 percent of $\bar{c}$. The plots of lift and pitching moment coefficients show the forward movement of vortex burst considerably reduced the lift and changed the characteristics of the pitching moment of the ACWFT1 planform at $\alpha = 30°$. Another change observed, compared to the previous flow-visualization figures, was that the wing vortex moved in the outboard direction to a position closely aligned with the wing leading edge, but the axial location of burst of the wing vortex remained nearly constant. The reason for the observed change in vortex position is that vortices with the same sense of rotation, clockwise or counterclockwise, tend to wrap around each other, leading to merging into a single vortex. Therefore, the wing vortex was drawn toward the forebody vortex at lower angles-of-attack. When the forebody vortex burst-point moved forward near the wing vortex at $\alpha = 30°$, the low-strength, burst forebody vortex had less influence on the wing vortex, and the wing vortex moved back near the wing leading edge. The movement of the wing vortex did not have as significant an effect on lift and pitching moment as did the location of vortex burst of the forebody vortex pair. Again, the side view shows that the height of the vortical flows above the model surface increases as α increases.

Figures 14a and 14b show the top and side view of the flow pattern over the ACWFT1 planform at $\alpha = 40°$. Again, the red and green dyes define the forebody vortex pair, and the photo shows that the longitudinal location of vortex burst of the forebody vortex pair has moved to a position that is approximately the midpoint of the forebody. The upstream movement of the vortex burst location still significantly reduces lift and influences the pitching moment at $\alpha = 40°$ (see figure 5 and 7). The asymmetric oscillation of the vortex burst location continued to occur at this α. The wing vortex (blue dye) has not significantly changed in character or location with the increase in α from 30° to 40°, but the axial location of vortex burst moved forward. The top view shows that the ACWFT1 planform was influenced by massive separation over most of the planform at $\alpha = 40°$. The side view photograph further shows the substantial region influenced by the vortex bursting.

Summary

A flat-plate wind tunnel model of an advanced fighter configuration (ACWFT) was tested in the NASA Langley Subsonic Basic Research Tunnel and the 16- by 24-Inch Water Tunnel. The ACWFT planform was the baseline planform for the integration of several innovative wing designs. The test objectives were to obtain and evaluate the longitudinal aerodynamic characteristics of the baseline planform, and a modified planform. Both planforms ACWFT1 and ACWFT2 were tested

over a range of freestream dynamic pressures from 15 psf to 30 psf (M = 0.07 to M = 0.14) and an angle-of-attack range from 0° to 40°. The data presented included the lift, induced drag and pitching moment coefficients for each planform, and flow-visualization photographs for the ACWFT1 planform. A comparison between experiment and linear theory was performed for the lift, induced drag and pitching moment of the ACWFT1 planform.

Lift and induced drag show little variation as a function of q_∞. Pitching moment shows little variation as a function of q_∞ for $\alpha \leq 15°$. The nonlinearities due to vortex flow were observed in the force and moment coefficient data. The comparison between experiment and linear theory showed good agreement for the lift and induced drag but poor agreement for the pitching moment. Linear theory did not agree at angles-of-attack dominated by vortex flow and the onset of vortex burst.

The flow-visualization photographs show the flow patterns over the ACWFT1 planform and provided insight to the aerodynamic nonlinearities due to vortex flow and vortex burst. At low angles-of-attack, the observed onset of vortex formation corresponded to the beginning of the nonlinear effects seen in the force and moment coefficient plots. For high angles-of-attack, the photographs show the presence and location of vortex burst which cause the highly nonlinear longitudinal aerodynamic characteristics. The presence and location of vortex burst over the planform considerably reduced lift and changed the longitudinal stability characteristics of the ACWFT1 planform.

The Test successfully defined the low-speed longitudinal aerodynamic characteristics of the ACWFT planform. This data was used for the design and integration of several innovative wing designs to an existing three-dimensional ACWFT wind tunnel model in preparation for future testing.

References

1. Pendergraft, O. C.; Neuhart, D. H.; and Kariya, T. T.: A User's Guide to the Langley 16- by 24-Inch Water Tunnel. NASA TM-104200, January 1992.

2. Carlson, H. W.; and Walkley, K. B.: A Computer Program for Wing Subsonic Aerodynamic Performance Estimates Inducing Attainable Thrust and Vortex Lift Effects. NASA CR-3515, March 1982.

3. Carlson, H. W.; and Darden, C. M.: Validation of a Pair of Computer Codes for Estimation and Optimization of Subsonic Aerodynamic Performance of Simple Hinged-Flap Systems for Thin Swept Wings. NASA TP-2828, November 1988.

4. Carlson, H. W.; Darden, C. M.; and Mann, M. J.: Validation of a Computer Code for Analysis of Subsonic Aerodynamic Performance of Wings with Flaps in Combination with a Canard or Horizontal Tail and an Application to Optimization . NASA TP-2961, January 1990.

5. Erickson, G. E.: Vortex Flow Correlation. AFWAL TR-80-3143, Final report for period May 1980 - October 1980, January 1981.

6. Erickson, G. E.: Flow Studies of Slender Wing Vortices. AIAA-80-1423, July 1980.

Table I. Wing geometric characteristics of the ACWFT flat plate wind tunnel and water tunnel model.

S	0.3784 sq. ft.
S_e	0.1946 sq. ft.
AR	2.65
λ	0.132
b	12.0 in.
c_r	8.0102 in.
c_t	1.0579 in.
$\bar{c}$	5.4445 in.
$\bar{c}_{LE}$	9.2320 in.
Λ_{LE}	30°
Λ_{TE}	30°

Table II. Test conditions for the ACWFT flat plate wind tunnel model in the Subsonic Basic Research Tunnel at the NASA Langley Research Tunnel.

q_∞ (psf)	M_∞	V_∞ (ft/sec)	V_∞ (mph)
7.5	0.071	80.2	54.7
15	0.101	113.5	77.4
30	0.142	160.5	109.4

Table III. Maximum loads and accuracy (0.3% of maximum loads) for balance SWT-01 with the ACWFT flat plate wind tunnel model at q_∞ = 30 psf.

Balance Channel	Load	Coefficient Accuracy
Normal	150 lbs.	± 0.0396
Axial	30 lbs.	± 0.0079
Pitch	225 in.-lbs.	± 0.0109

Table IV. Wind tunnel force and moment data of the ACWFT flat plate model.

(a) ACWFT1, Run 1, q_∞ = 30 psf

α	q_∞(psf)	C_L	C_D	C_A	C_N	C_m	$C_{D,i}$
0	30.03	-0.0750	0.0370	0.0370	-0.0750	0.0309	0.0000
5	30.00	0.2315	0.0585	0.0381	0.2357	0.0650	0.0215
10	29.68	0.5365	0.1370	0.0418	0.5521	0.1004	0.1000
15	29.67	0.8850	0.2850	0.0462	0.9286	0.1589	0.2480
20	30.29	1.2740	0.5250	0.0576	1.3767	0.2313	0.4880
25	29.84	1.5887	0.8223	0.0738	1.7874	0.2604	0.7853
30	29.94	1.7260	1.0975	0.0875	2.0435	0.2492	1.0605
35	29.94	1.7373	1.3357	0.0977	2.1892	0.2511	1.2987
40	30.09	1.6967	1.5650	0.1082	2.3057	0.2394	1.5280

(b) ACWFT1, Run 2, q_∞ = 15 psf

α	q_∞(psf)	C_L	C_D	C_A	C_N	C_m	$C_{D,i}$
0	14.98	-0.0730	0.0480	0.0480	-0.0730	0.0287	0.0000
5	14.94	0.2095	0.0640	0.0455	0.2143	0.0593	0.0160
10	14.95	0.5080	0.1335	0.0433	0.5235	0.0988	0.0855
15	14.95	0.8430	0.2660	0.0388	0.8831	0.1564	0.2180
20	15.02	1.2185	0.4880	0.0418	1.3119	0.2224	0.4400
25	15.02	1.5400	0.7720	0.0488	1.7220	0.2477	0.7240
30	15.11	1.7035	1.0470	0.0550	1.9988	0.2388	0.9990
35	14.96	1.7513	1.3033	0.0631	2.1821	0.2435	1.2553
40	15.14	1.7193	1.5370	0.0723	2.3050	0.2222	1.4890

(c) ACWFT1, Run 3, q_∞ = 7.5 psf

α	q_∞(psf)	C_L	C_D	C_A	C_N	C_m	$C_{D,i}$
0	7.68	-0.0820	0.0510	0.0510	-0.0820	0.0394	0.0000
5	7.68	0.1965	0.0685	0.0511	0.2017	0.0650	0.0175
10	7.59	0.4845	0.1310	0.0449	0.4999	0.1003	0.0800
15	7.51	0.7990	0.2520	0.0366	0.8370	0.1588	0.2010
20	7.61	1.1705	0.4555	0.0277	1.2557	0.2126	0.4045
25	7.72	1.4883	0.7233	0.0265	1.6545	0.2488	0.6723
30	7.41	1.6820	0.9980	0.0233	1.9557	0.2360	0.9470
35	7.51	1.7385	1.2565	0.0321	2.1448	0.2412	1.2055
40	7.63	1.7037	1.4770	0.0363	2.2545	0.2182	1.4260

Table IV. Concluded.

(d) ACWFT2, Run 4, q_∞ = 30 psf

α	q_∞(psf)	C_L	C_D	C_A	C_N	C_m	$C_{D,i}$
0	30.16	-0.0765	0.0315	0.0315	-0.0765	0.0397	0.0000
5	29.83	0.2205	0.0565	0.0371	0.2246	0.0749	0.0250
10	30.03	0.5265	0.1350	0.0415	0.5419	0.1272	0.1035
15	30.00	0.8715	0.2810	0.0459	0.9145	0.1929	0.2495
20	29.92	1.2425	0.5125	0.0566	1.3429	0.2701	0.4810
25	29.97	1.5320	0.7945	0.0726	1.7242	0.3153	0.7630
30	29.93	1.6270	1.0375	0.0850	1.9278	0.3358	1.0060
35	30.03	1.6410	1.2685	0.0979	2.0718	0.3638	1.2370
40	29.98	1.5770	1.4640	0.1078	2.1491	0.3716	1.4325

Table V. Estimation of the linear aerodynamic characteristics from the SBRT test of the ACWFT configurations.

Run	Config.	$C_{L\alpha}$ (per deg.)	$C_{m\alpha}$ (per deg.)	dC_m/dC_L	$C_{D,0}$
1	ACWFT1	0.0612	0.0069	0.1102	0.0369
2	ACWFT1	0.0581	0.0070	0.1025	0.0475
3	ACWFT1	0.0567	0.0061	0.0857	0.0517
4	ACWFT2	0.0594	0.0070	0.1058	0.0331

Table VI. Estimation of the linear aerodynamic characteristics from linear theory of the ACWFT1 configuration.

Linear Theory	$C_{L\alpha}$ (per deg.)	$C_{m\alpha}$ (per deg.)	dC_m/dC_L
No Thrust	0.053	0.0045	0.085
Full Thrust	0.053	0.0045	0.085
Attainable Thrust	0.055	0.0053	0.096

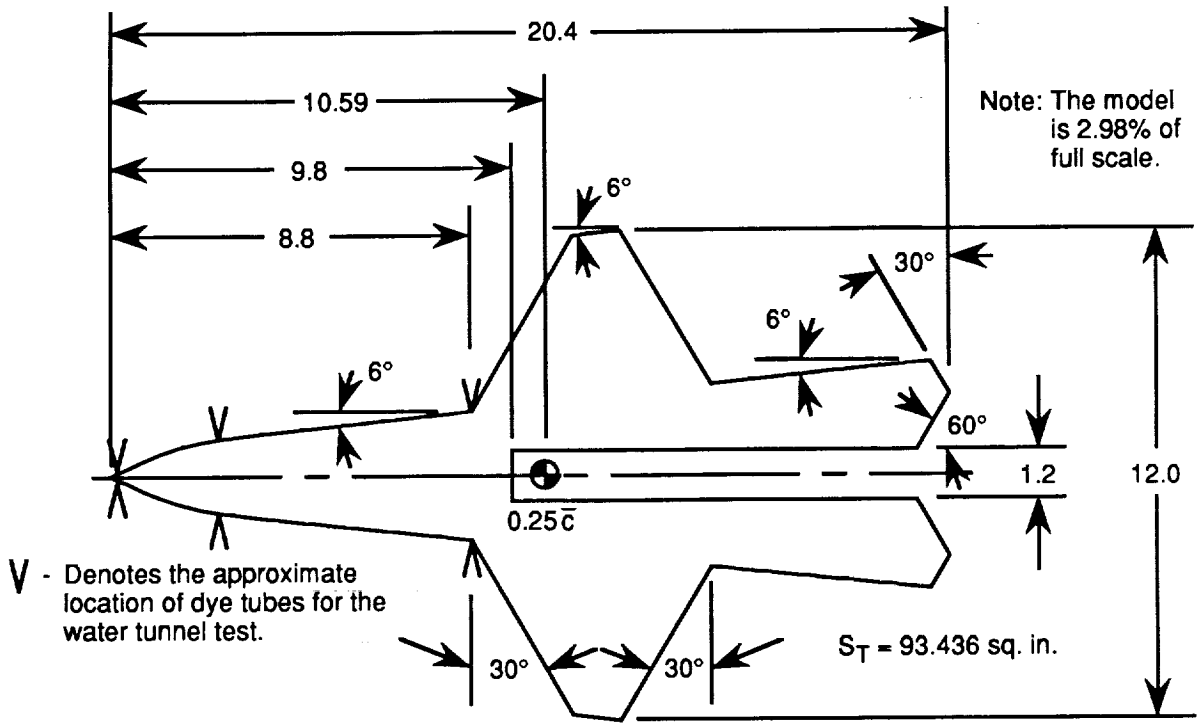

(a) ACWFT1

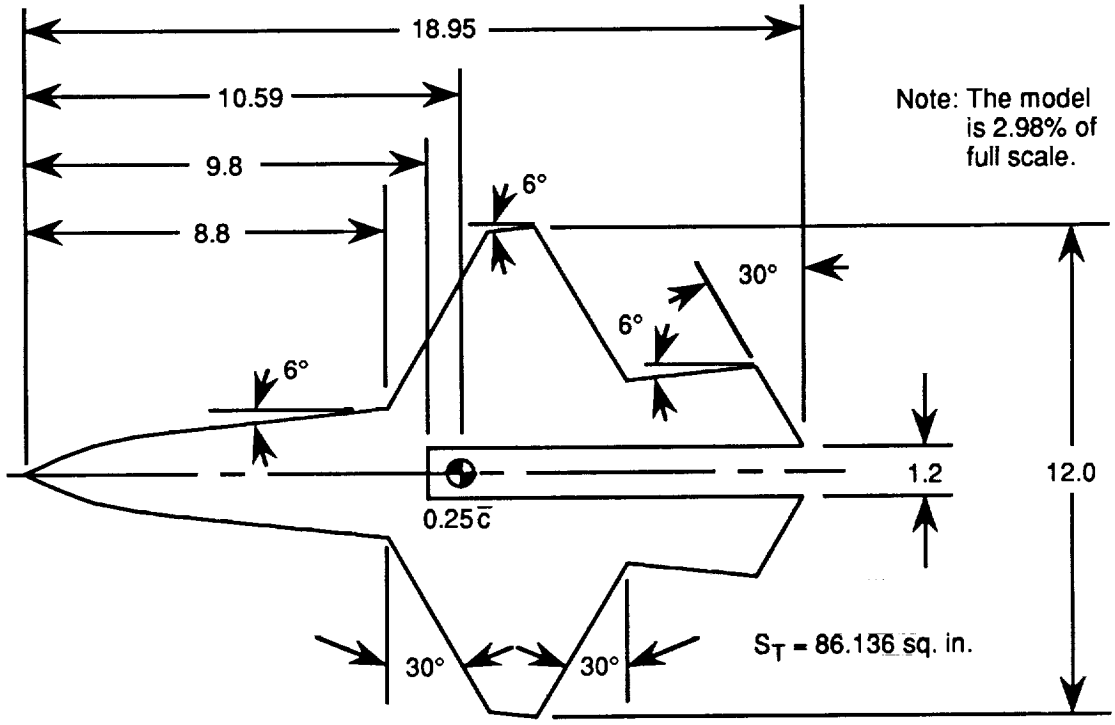

(b) ACWFT2

Figure 1. Geometry of the ACWFT flat plate wind tunnel and water tunnel model. All dimensions are in inches.

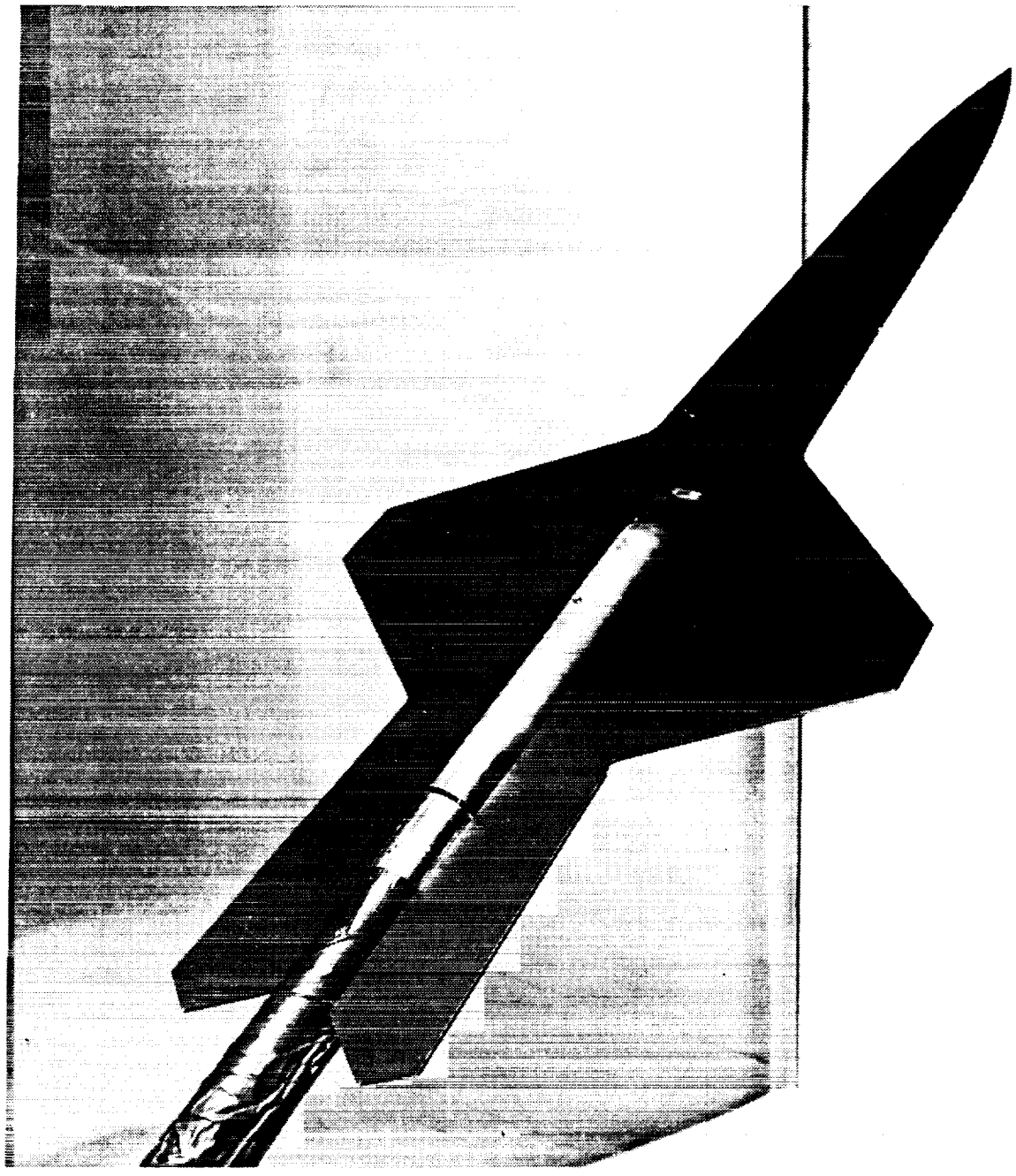

Figure 2. ACWFT1 configuration in the Subsonic Basic Research Tunnel at the NASA Langley Research Center.

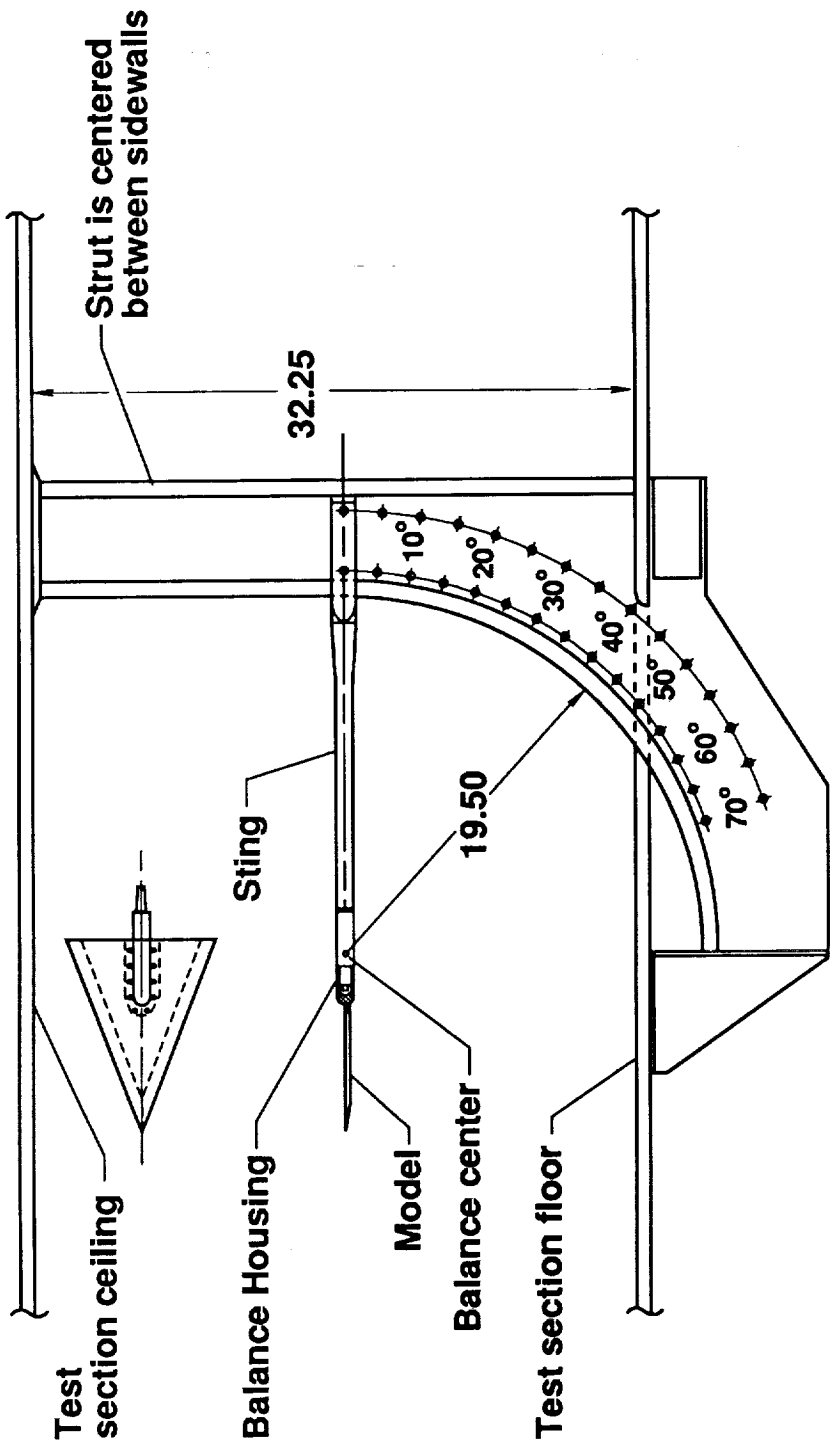

Figure 3. Model support system for the Subsonic Basic Research Tunnel at the NASA Langley Research Center. All dimensions are in inches.

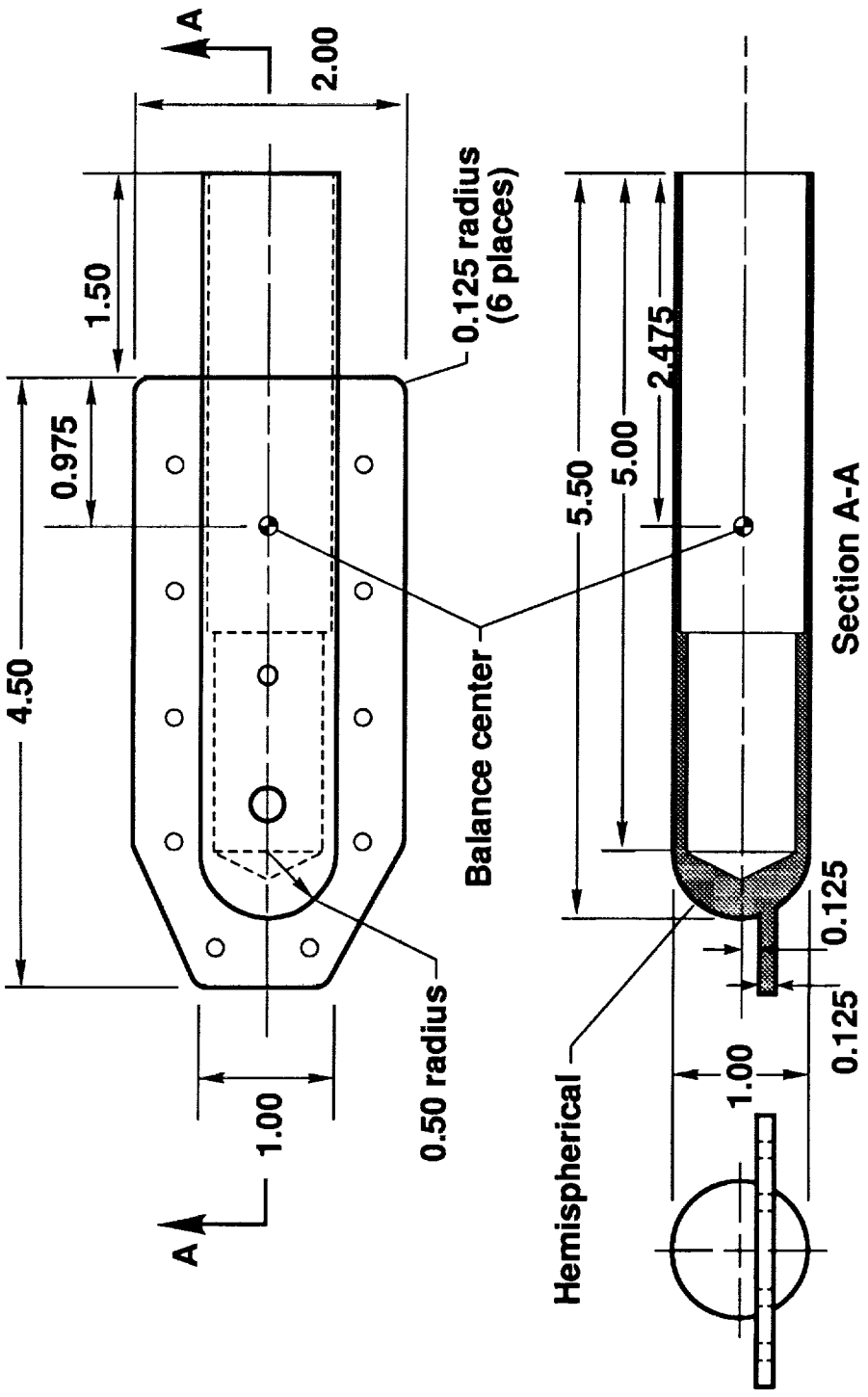

Figure 4. Model balance housing for the Subsonic Basic Research Tunnel at the NASA Langley Research Center. All dimensions are in inches.

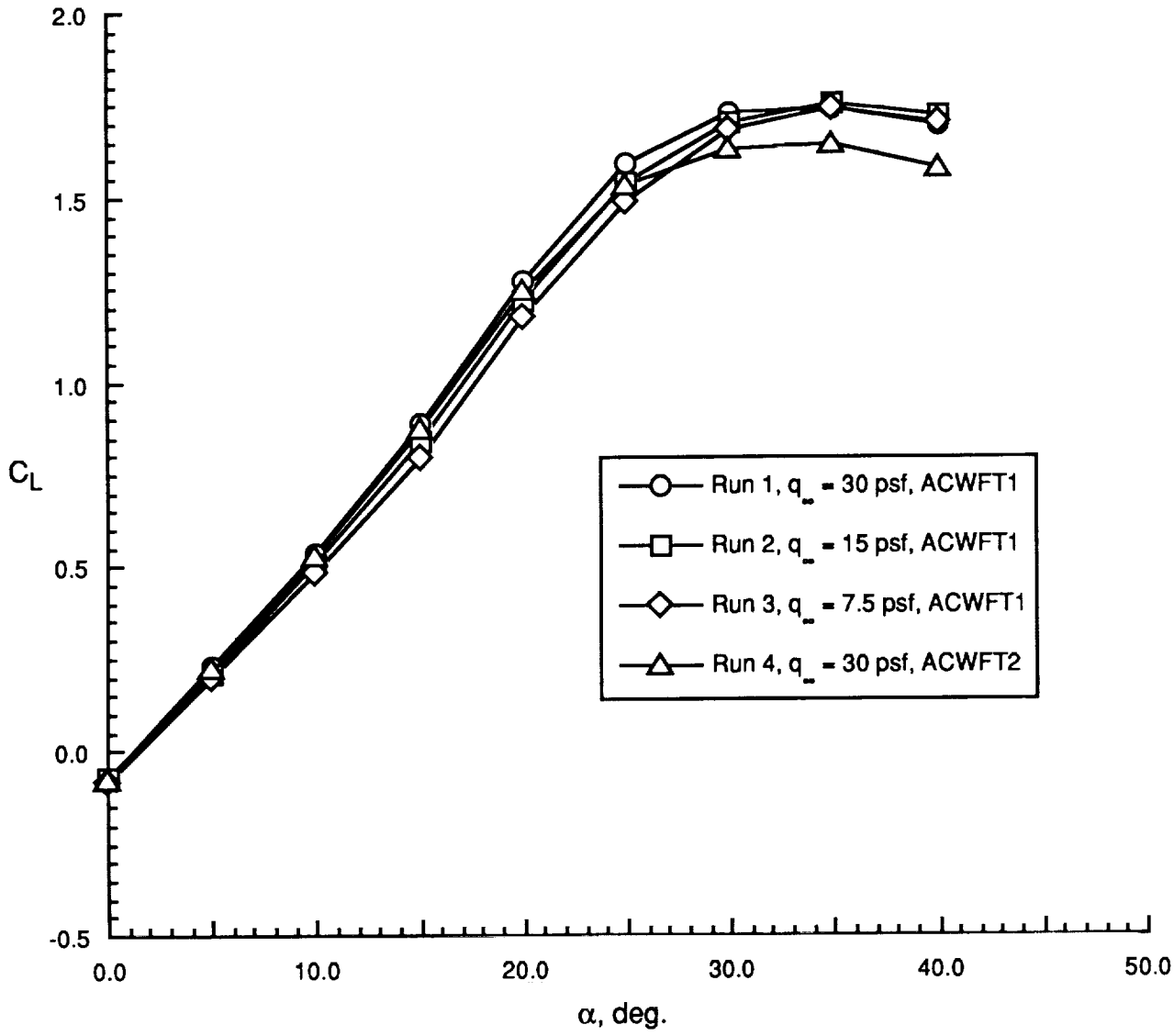

Figure 5. Lift coefficient as a function of α and q_∞ for the ACWFT configurations.

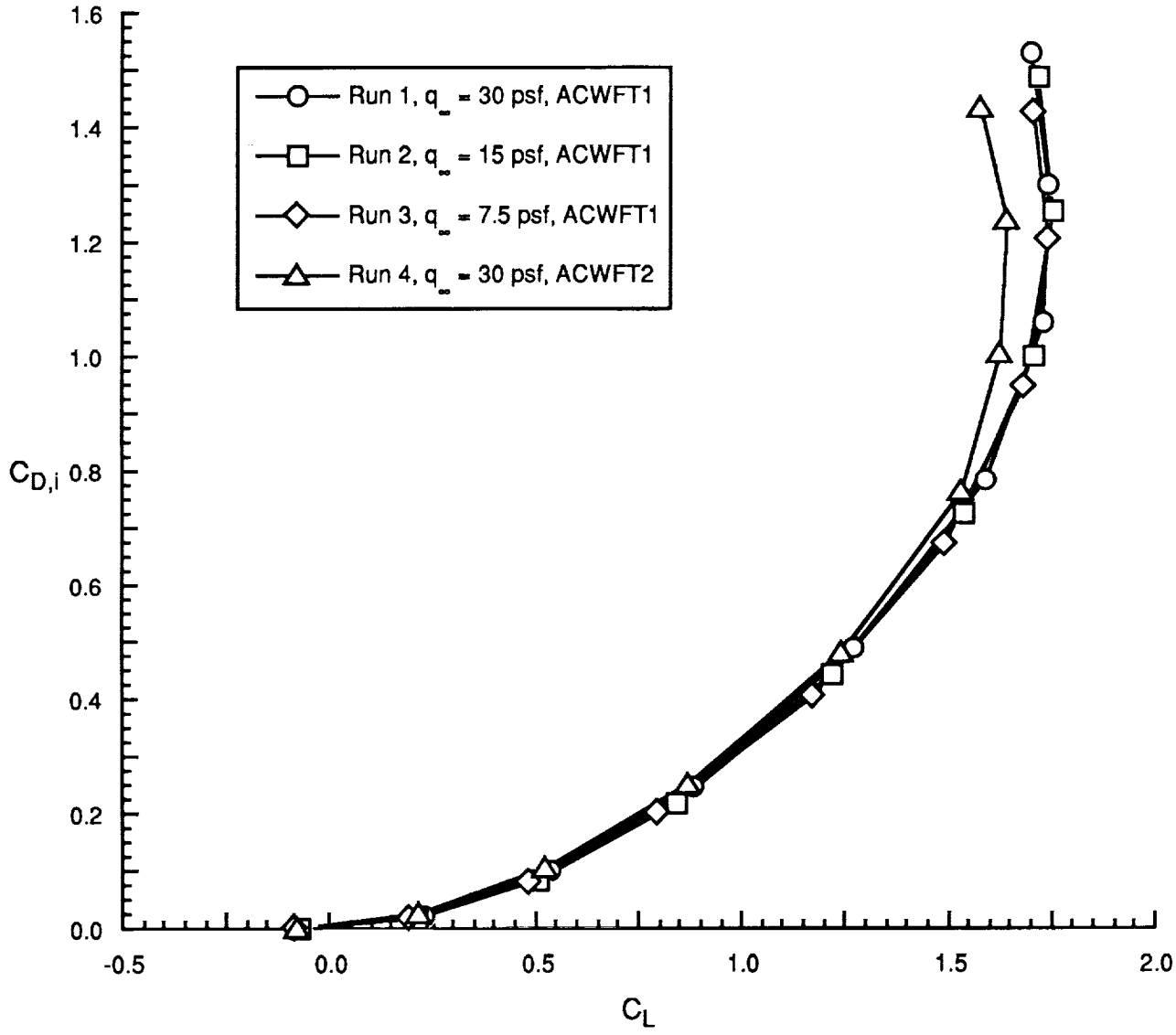

Figure 6. Induced drag coefficient as a function of C_L and q_∞ for the ACWFT configurations.

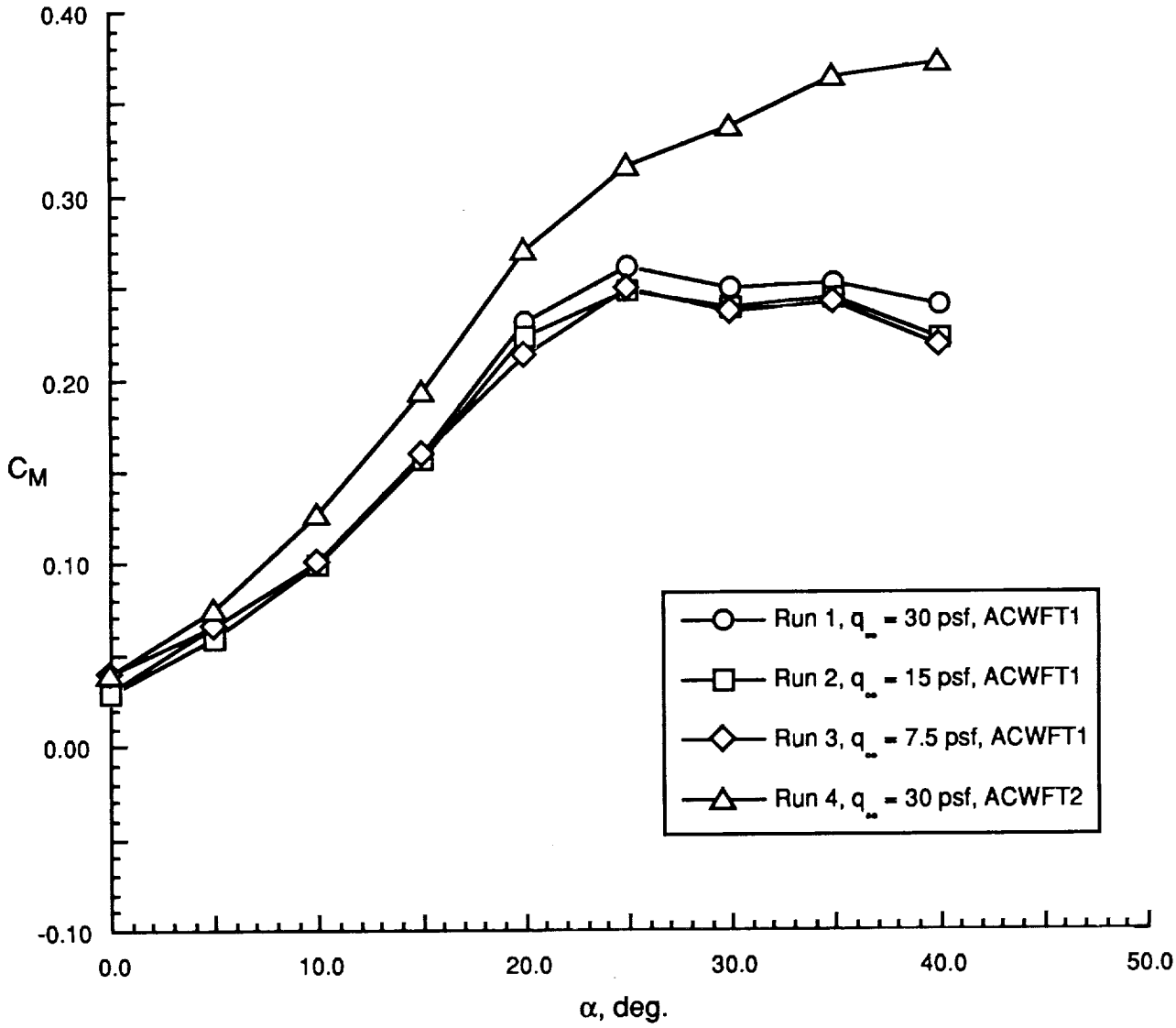

Figure 7. Pitching moment coefficient as a function of α and q_∞ for the ACWFT configurations.

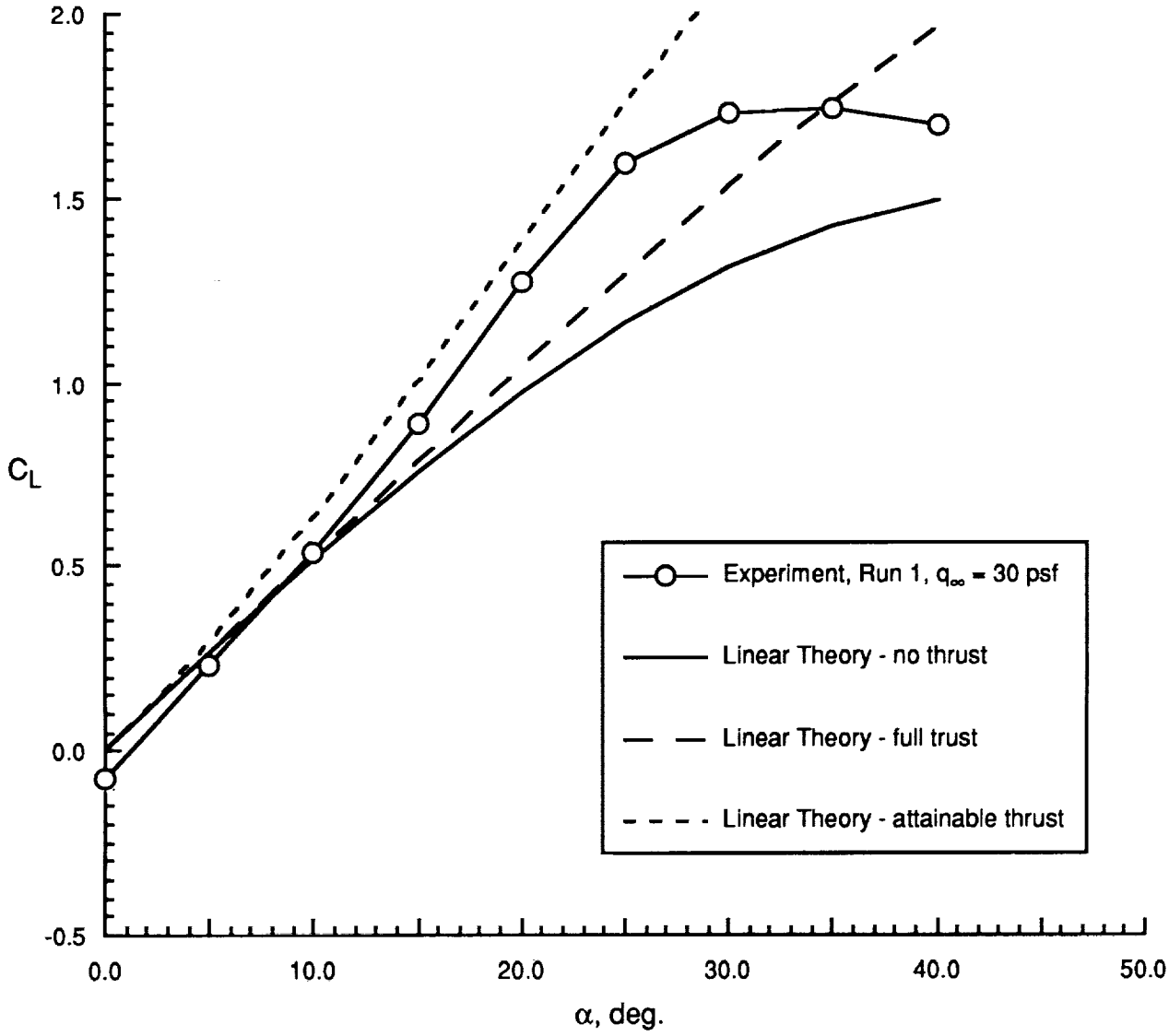

Figure 8. Comparison between SBRT and linear theory of the lift coefficient for the ACWFT1 configuration.

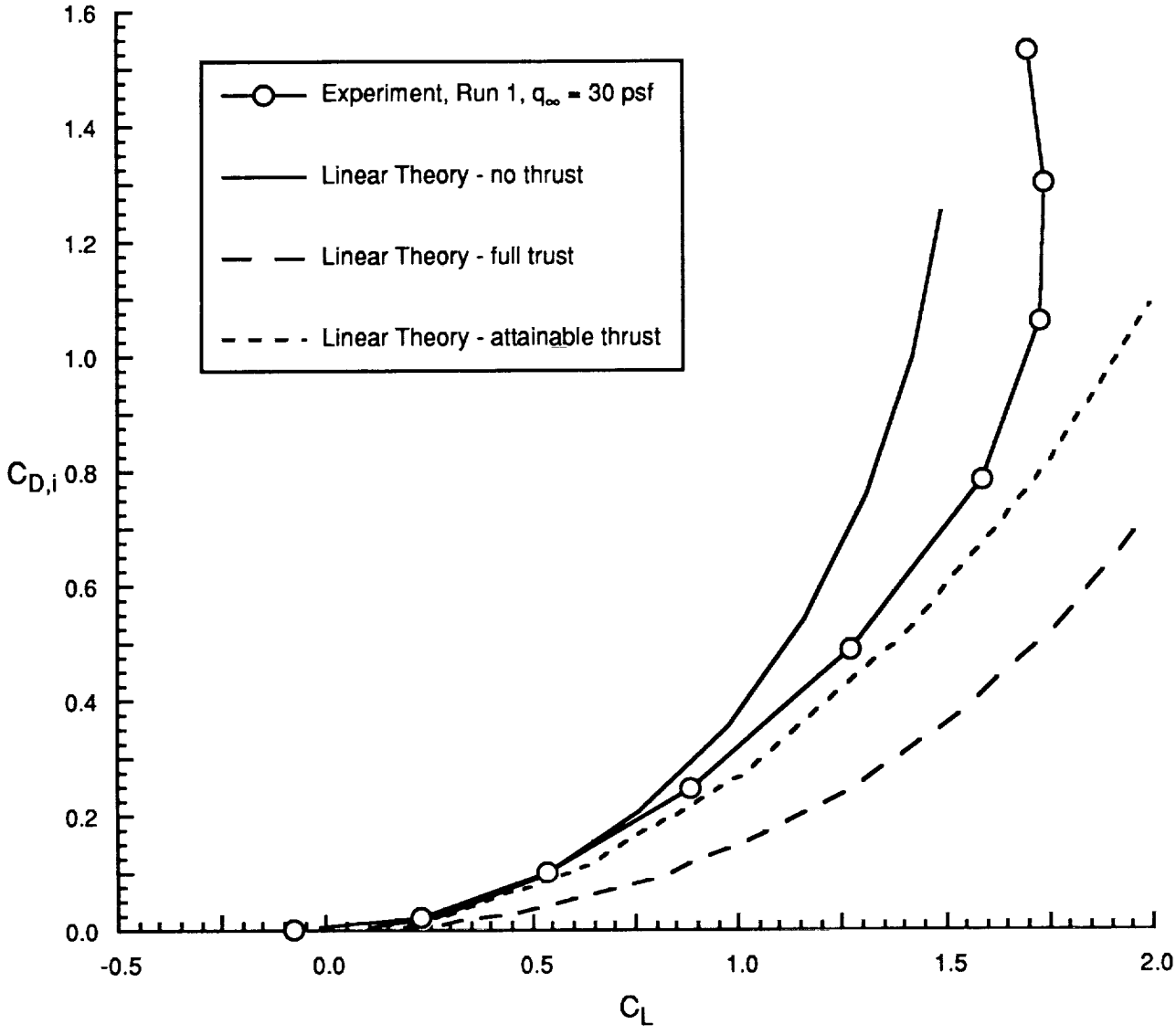

Figure 9. Comparison between SBRT and linear theory of the induced drag coefficient for the ACWFT1 configuration.

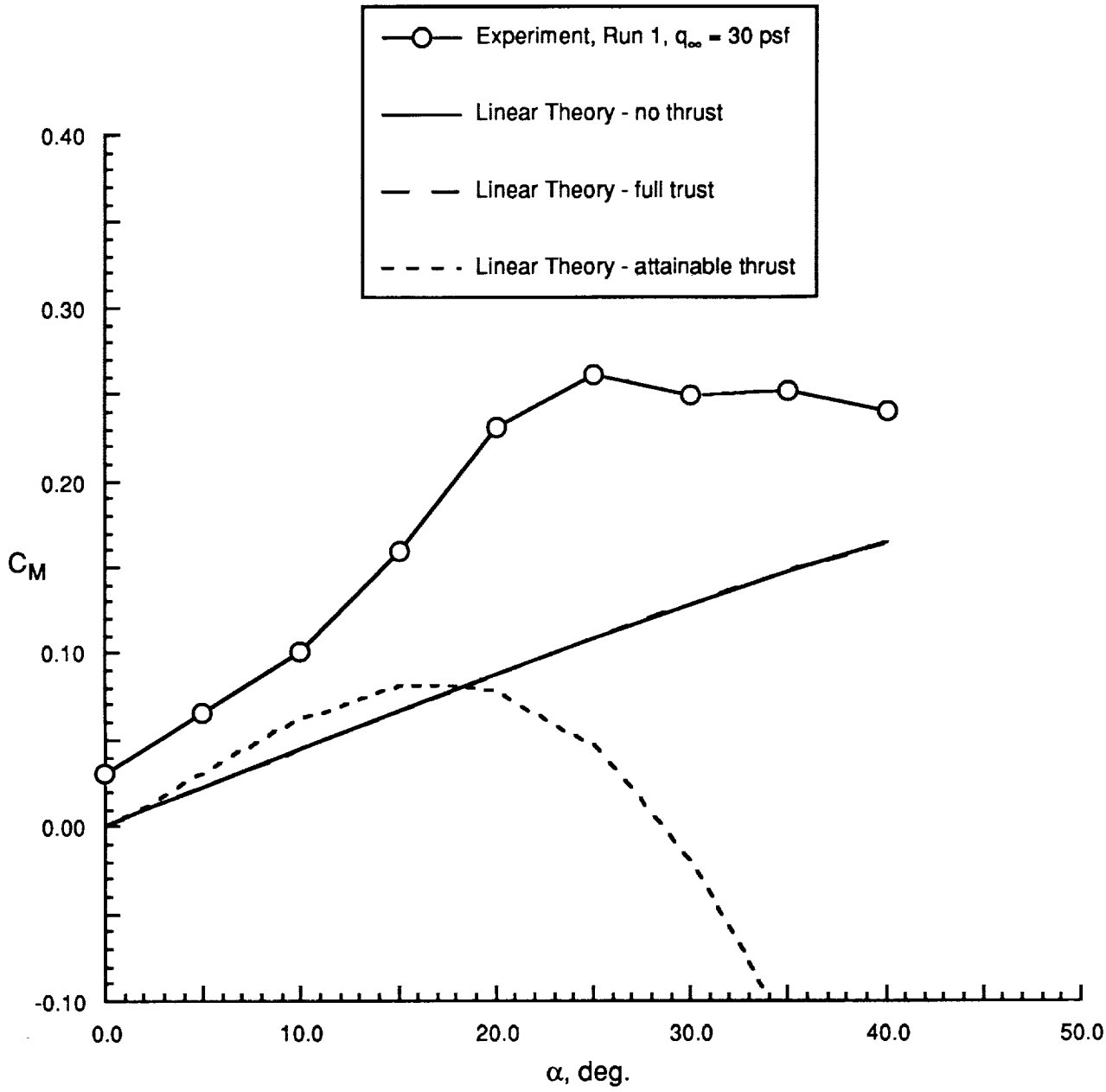

Figure 10. Comparison between SBRT and linear theory of the pitching moment coefficient for the ACWFT1 configuration.

ORIGINAL PAGE
COLOR PHOTOGRAPH

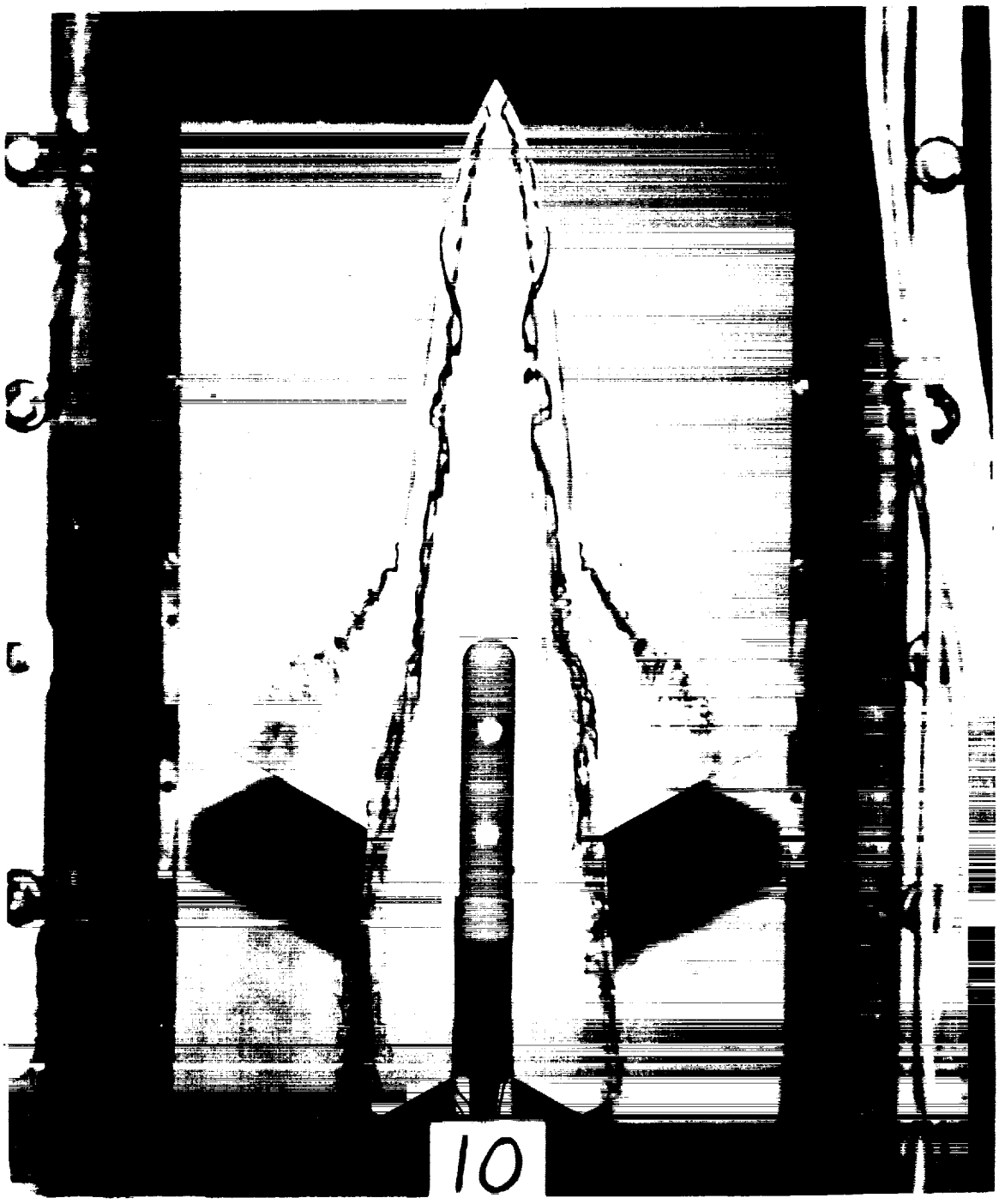

(a) Top view

Figure 11. Water tunnel results for the ACWFT1 configuration at $\alpha = 10°$.

ORIGINAL PAGE
COLOR PHOTOGRAPH

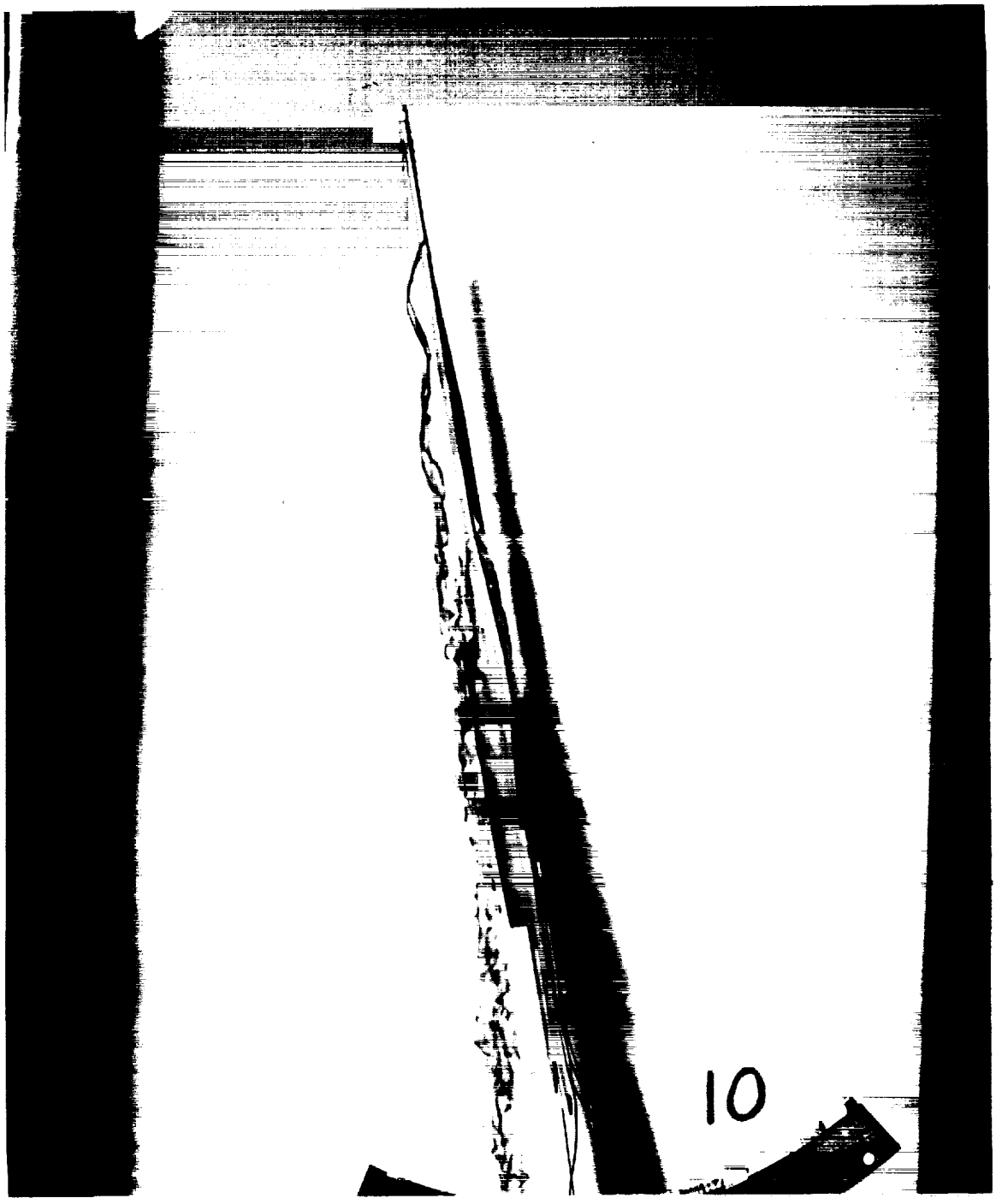

(b) Side view

Figure 11. Concluded.

ORIGINAL PAGE
COLOR PHOTOGRAPH

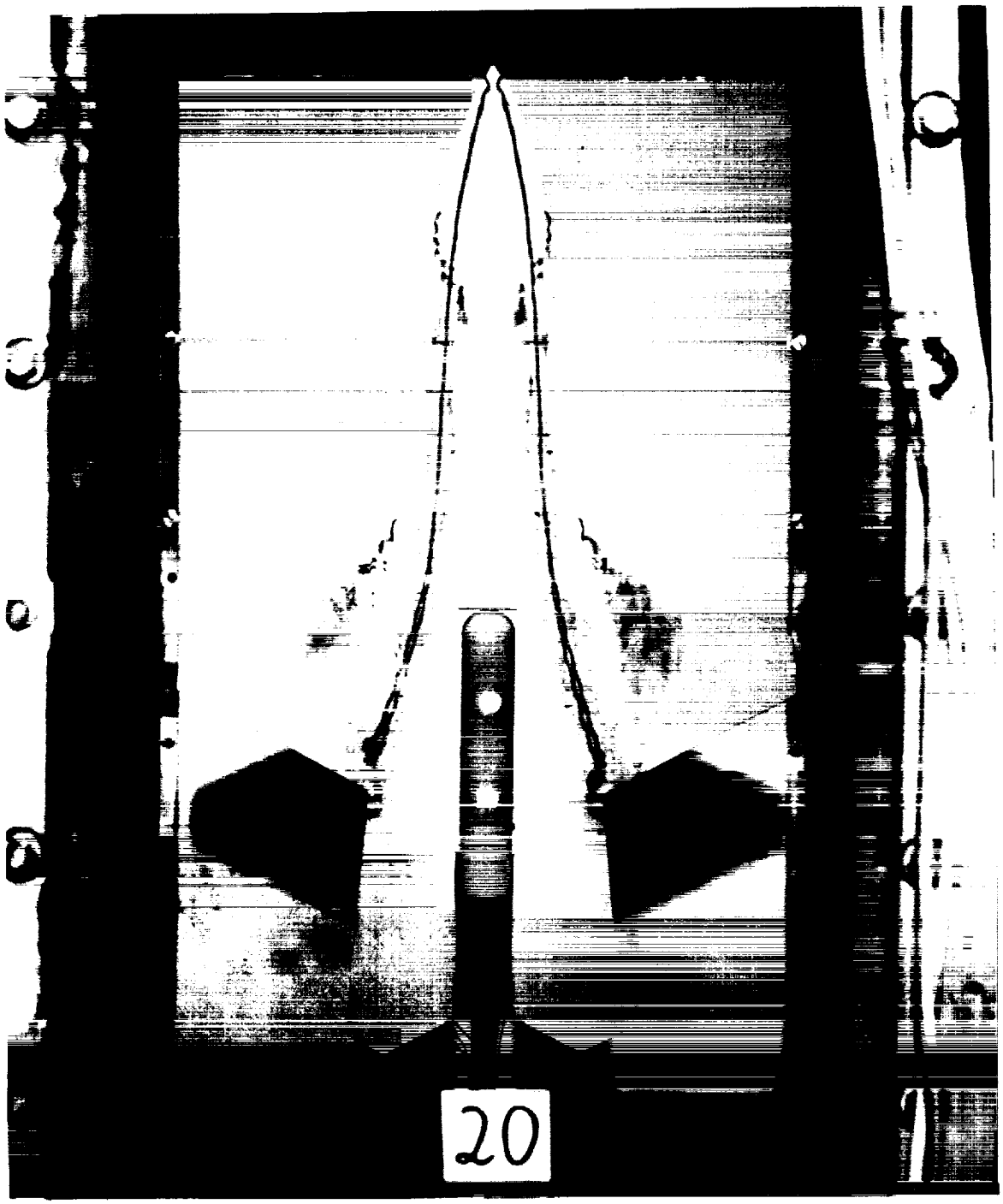

(a) Top view

Figure 12. Water tunnel results for the ACWFT1 configuration at $\alpha = 20°$.

ORIGINAL PAGE
COLOR PHOTOGRAPH

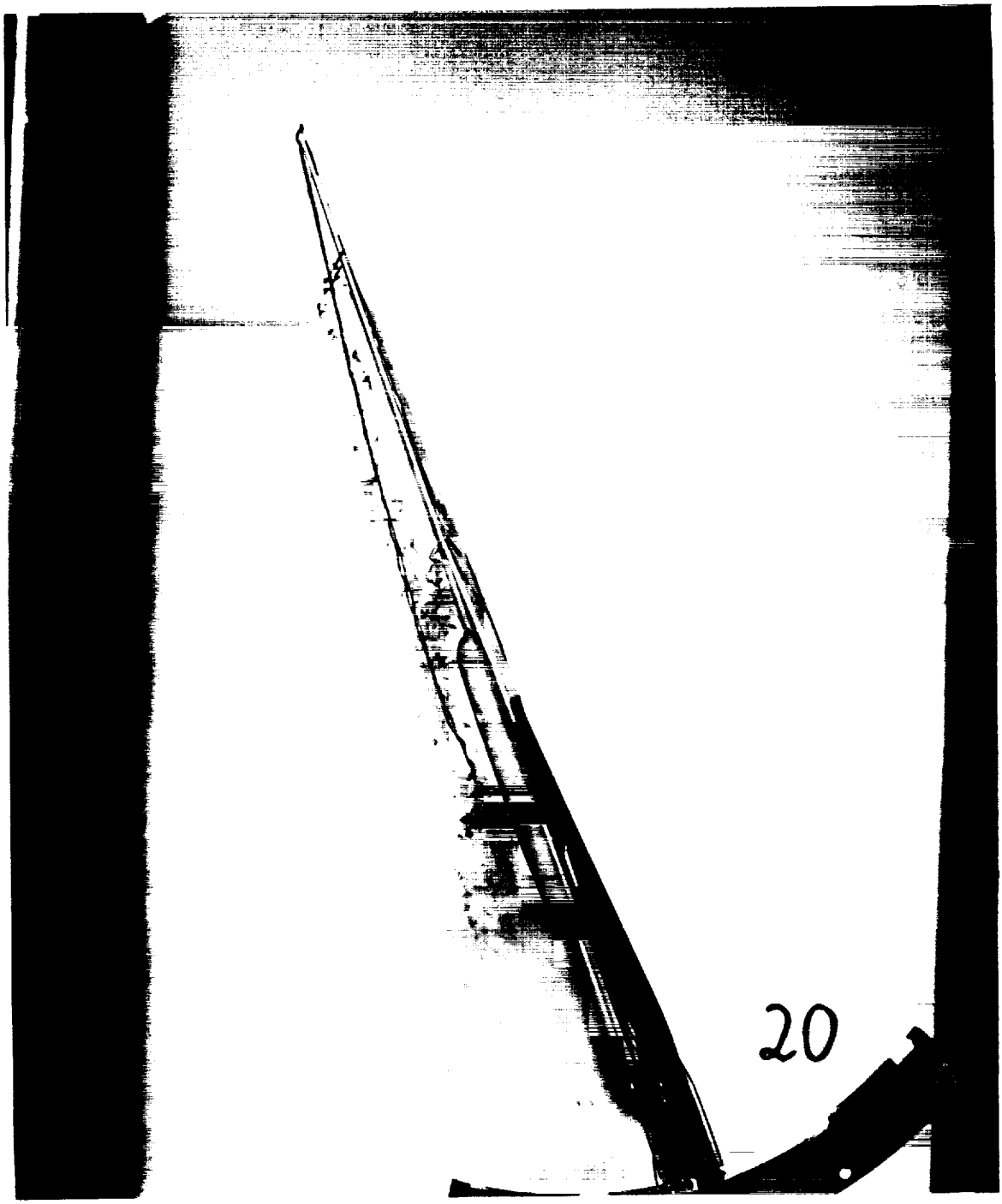

(b) Side view

Figure 12. Concluded.

ORIGINAL PAGE
COLOR PHOTOGRAPH

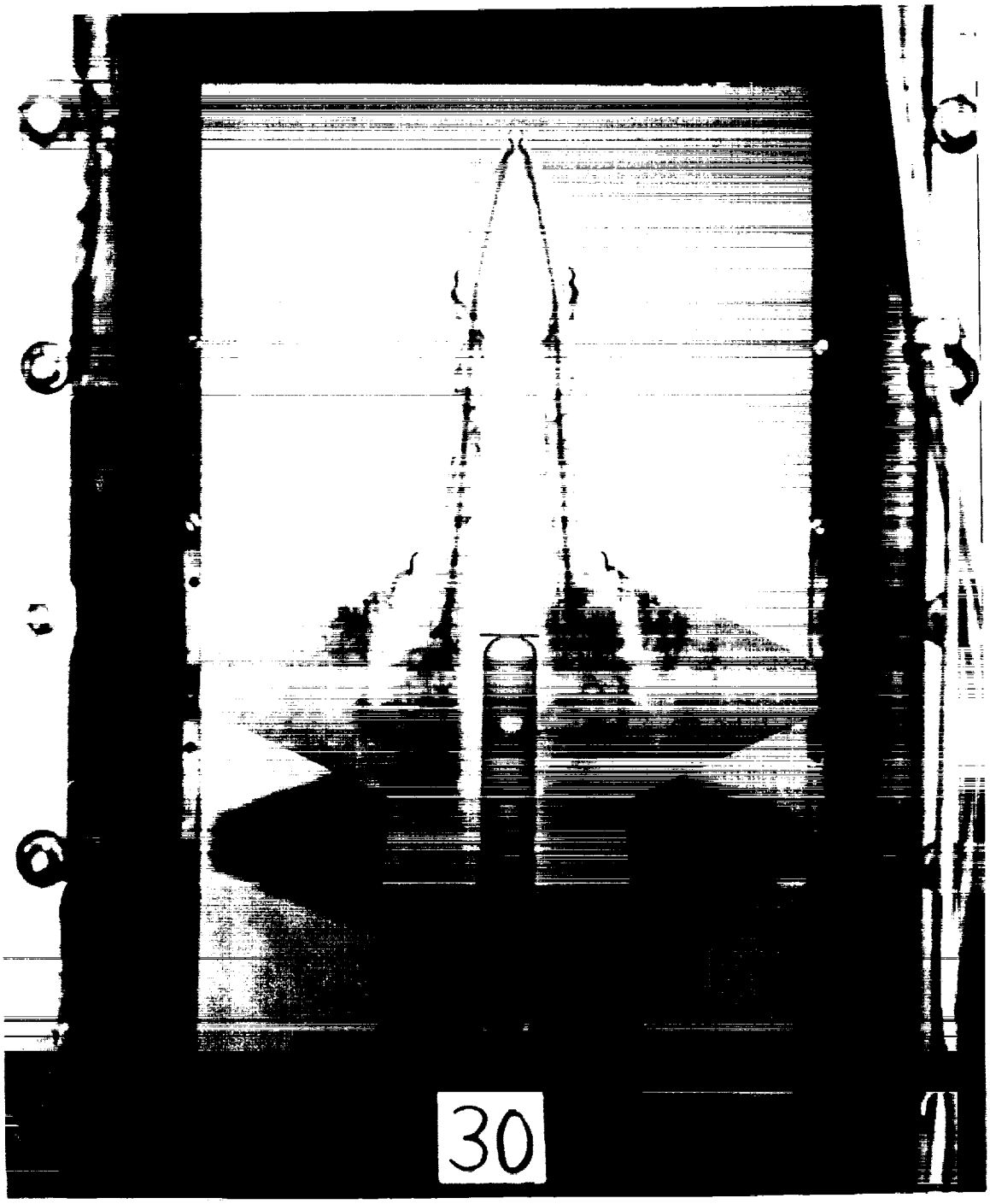

(a) Top view

Figure 13. Water tunnel results for the ACWFT1 configuration at α = 30°.

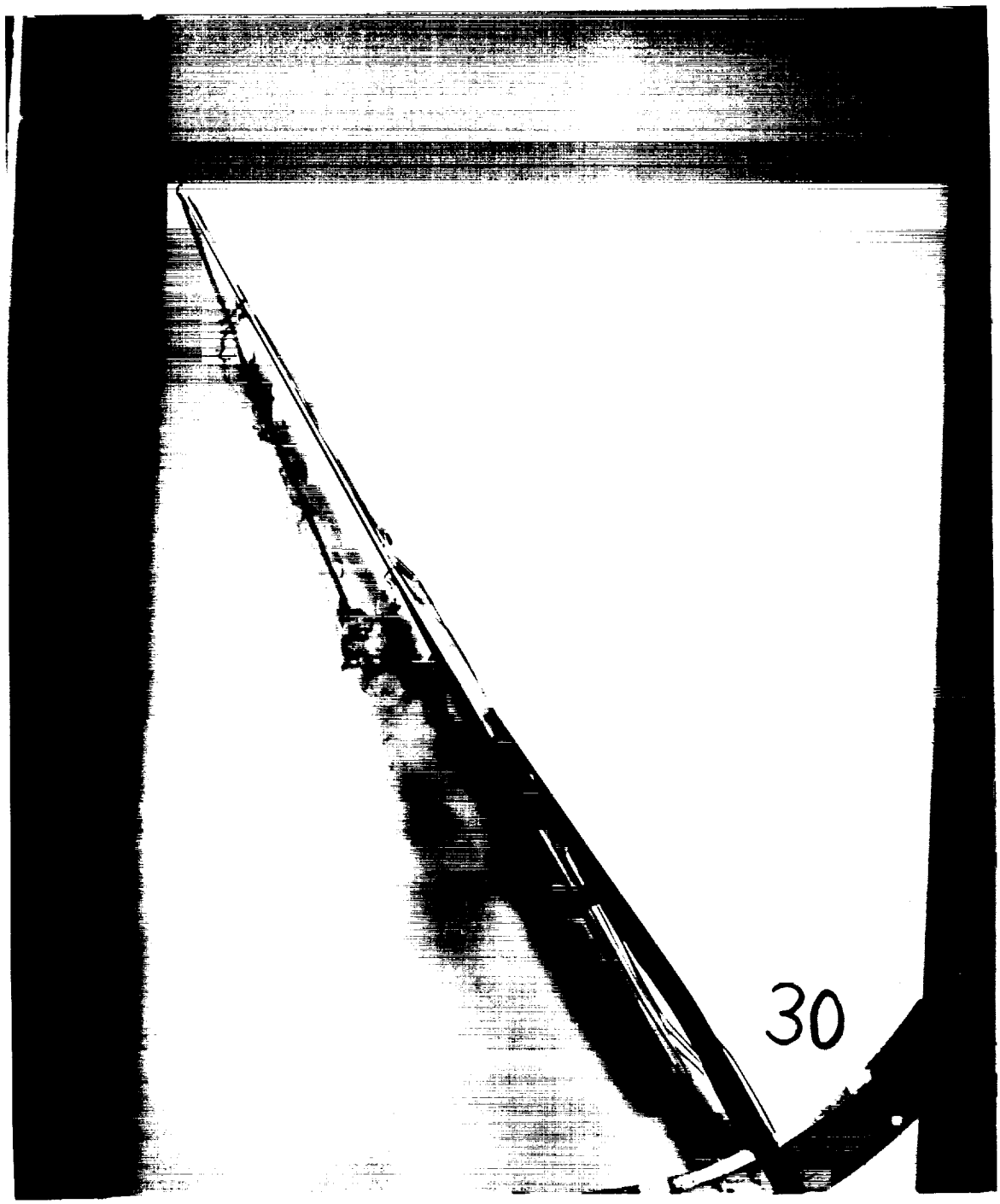

(b) Side view

Figure 13. Concluded.

ORIGINAL PAGE
COLOR PHOTOGRAPH

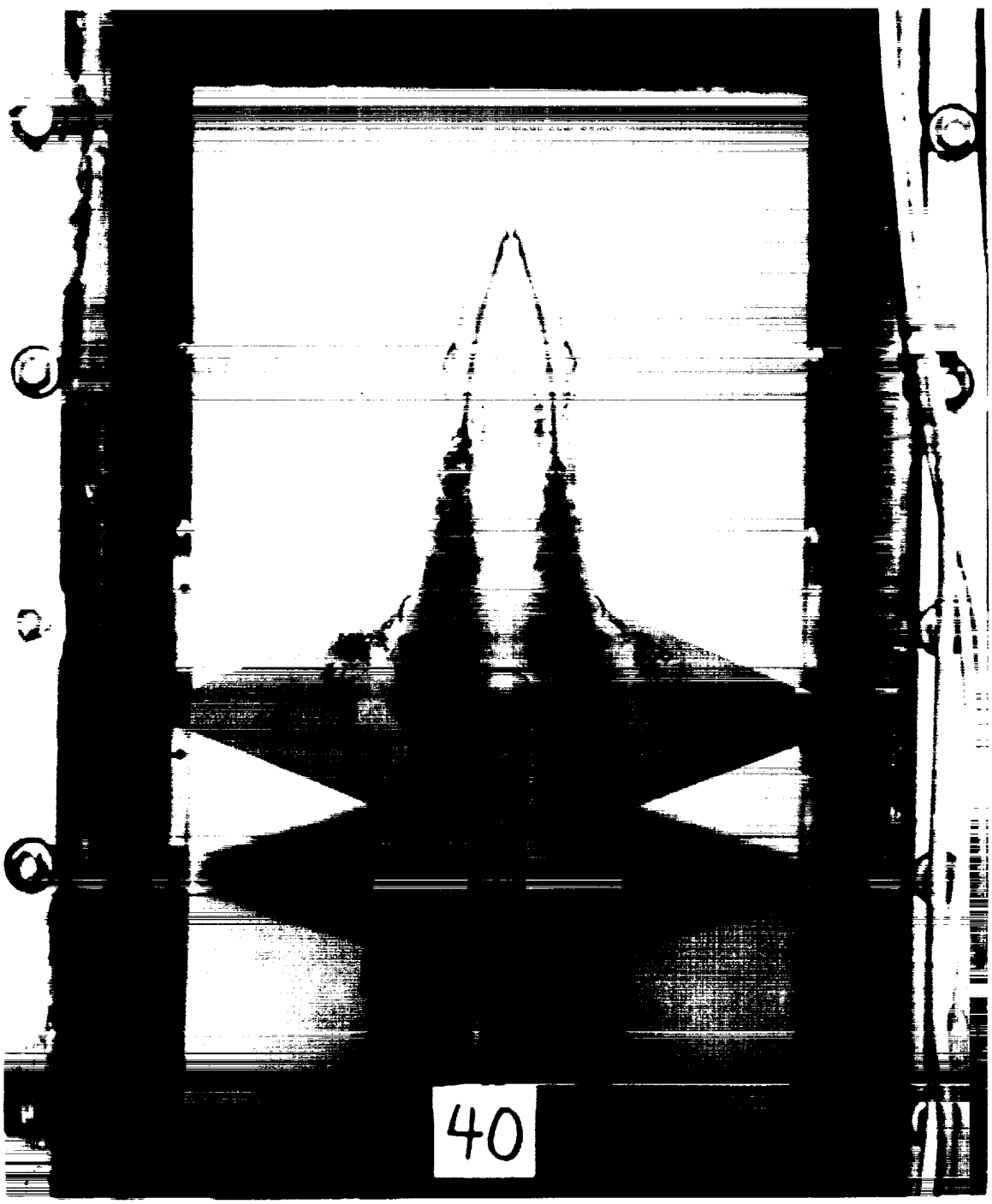

(a) Top view

Figure 14. Water tunnel results for the ACWFT1 configuration at $\alpha = 40°$.

ORIGINAL PAGE
COLOR PHOTOGRAPH

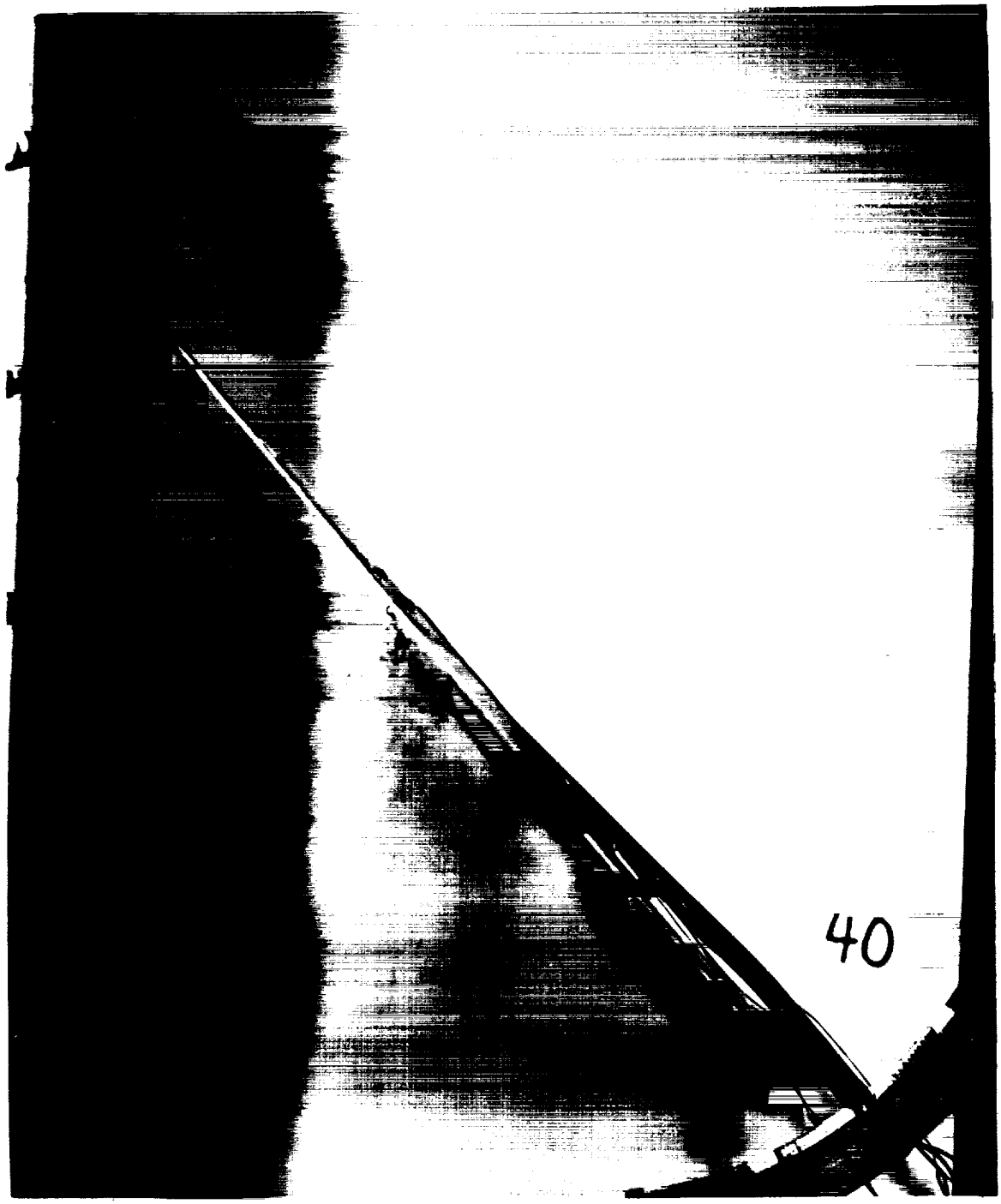

(b) Side view

Figure 14. Concluded.

REPORT DOCUMENTATION PAGE

Form Approved
OMB No. 0704-0188

1. AGENCY USE ONLY *(Leave blank)*	2. REPORT DATE	3. REPORT TYPE AND DATES COVERED
	March 1994	Technical Memorandum

4. TITLE AND SUBTITLE
Low-Speed Longitudinal Aerodynamic Characteristics of a Flat Plate Planform Model of an Advanced Fighter Configuration

5. FUNDING NUMBERS
505-68-70-05

6. AUTHOR(S)
Brian E. McGrath, Dan H. Neuhart, Gregory M. Gatlin, and Pat O'Neil

7. PERFORMING ORGANIZATION NAME(S) AND ADDRESS(ES)
NASA Langley Research Center
Hampton, VA 23681-0001

8. PERFORMING ORGANIZATION REPORT NUMBER

9. SPONSORING / MONITORING AGENCY NAME(S) AND ADDRESS(ES)
National Aeronautics and Space Administration
Washington, DC 20546-0001

10. SPONSORING / MONITORING AGENCY REPORT NUMBER
NASA TM-109045

11. SUPPLEMENTARY NOTES
McGrath and Neuhart: Lockheed Engineering and Sciences Co. Hampton, VA
Gatlin: Langley Research Center, Hampton, VA
O'Neil: McDonnell Douglas Aerospace, St. Louis, MO

12a. DISTRIBUTION / AVAILABILITY STATEMENT
Unclassified-Unlimited
Subject Category 02

12b. DISTRIBUTION CODE

13. ABSTRACT *(Maximum 200 words)*
A flat-plate wind tunnel model of an advanced fighter configuration was tested in the NASA Langley Subsonic Basic Research Tunnel and the 16- by 24-Inch Water Tunnel. The test objectives were to obtain and evaluate the low-speed longitudinal aerodynamic characteristics of a candidate configuration for the integration of several new innovative wing designs. The flat plate test allowed for the initial evaluation of the candidate planform and was designated as the baseline planform for the innovative wing design study. Low-speed longitudinal aerodynamic data were obtained over a range of freestream dynamic pressures from 7.5 psf to 30 psf (M= 0.07 to M = 0.14) and angles-of-attack from 0° to 40°. The aerodynamic data are presented in coefficient form for the lift, induced drag and pitching moment. Flow-visualization results obtained were photographs of the flow pattern over the flat plate model in the water tunnel for angles-of-attack from 10° to 40°. The force and moment coefficients and the flow-visualization photographs showed the linear and nonlinear aerodynamic characteristics due to attached flow and vortical flow over the flat plate model. Comparison between experiment and linear theory showed good agreement for the lift and induced drag; however, the agreement was poor for the pitching moment.

14. SUBJECT TERMS	15. NUMBER OF PAGES
Subsonic aerodynamic characteristics; water tunnel testing; advanced fighter aerodynamics; wind tunnel testing	35
	16. PRICE CODE A03

17. SECURITY CLASSIFICATION OF REPORT	18. SECURITY CLASSIFICATION OF THIS PAGE	19. SECURITY CLASSIFICATION OF ABSTRACT	20. LIMITATION OF ABSTRACT
Unclassified	Unclassified	Unclassified	

NSN 7540-01-280-5500

Standard Form 298 (Rev. 2-89)
Prescribed by ANSI Std. Z39-18
298-102